Identification of RF Devices Through Constellation Patterns Using Complex-Valued Neural Networks

Yoshihiro Kitagawa*, Kakuto Goto*, Tomotaka Kimura*, and Jun Cheng*
* Department of Intelligent Information Engineering and Sciences, Doshisha University, Kyoto 610-0321, Japan
(e-mail: ctwj0121@mail4.doshisha.ac.jp; ctwk0112@mail4.doshisha.ac.jp; tomkimur@mail.doshisha.ac.jp; jcheng@ieee.org)

***Abstract*—Complex-valued neural network (CvNN)-based device identification is proposed to enhance the security of communications. Devices have in-phase/quadrature (I/Q) impairments that arise from variations in the manufacturing process. An access point (AP) receives I/Q symbols from a device and forms a constellation pattern, which has a unique feature of the device's inherent I/Q impairments. The CvNN is able to recognize the device by categorizing the pattern. Simulations demonstrate that the CvNN has a lower error rate in identification than a real-valued neural network. This is because the CvNN captures the inherent correlation in complex-valued I/Q symbols caused by I/Q imbalances.**

***Index Terms*—I/Q imbalances, RF device identification, constellation pattern, complex value neural network**

I. Introduction

In wireless communication systems, various frequency bands are chosen as carriers based on the system requirements. RF (radio frequency) circuits within an RF transmitter play a crucial role by modulating the baseband signal to these RF frequency bands during transmission. Historically, the superheterodyne approach was prevalent; in this approach, the baseband signal is initially transformed to an intermediate frequency (IF) for processing before being shifted to an RF signal. This approach was favored because it provided stability in the functionality of components such as filters and amplifiers.

In contrast, the direct conversion (DC) approach, which allows the baseband signal to be directly transformed into the RF signal bypassing any IF, has gained popularity. This is due to the elimination of the necessity for IF processing circuits, which considerably minimizes the circuit dimensions. The DC approach is particularly well suited for IoT devices (Internet of Things), which aim to optimize cost, minimize physical size, and reduce power usage. The surge in the number of communication-capable devices, driven by the widespread adoption of 5G and IoT [1], has further heightened its relevance.

However, the efficient hardware and architecture of IoT devices implemented in DC applications are susceptible to the effects of I/Q imbalances, a type of RF impairment caused by manufacturing variations. In a modulator, I/Q imbalances refer to mismatches between the in-phase (I) and quadrature (Q) signal paths, which are supposed to be orthogonal. These imbalances typically result from amplitude and phase distortion. I/Q imbalances are inherent to hardware, making it difficult to completely eliminate, even with advanced manufacturing technologies, and similarly challenging to manipulate. For this reason, I/Q imbalances are utilized for device identification to ensure the security of IoT communications [2]. Note that the distortion caused by I/Q imbalances is minimal and does not significantly affect regular wireless communications.

In RF-based device identification methods, experts select identifiable physical features to confirm the identity of devices [3] [4] [5]. However, neural networks (NNs) can learn appropriate features for device identification in a data-driven manner. Most NN-based identification methods use raw RF I/Q samples as input [6] [7], as various RF imperfections, including I/Q imbalances, are observable in RF I/Q waveforms [8]. Since I/Q imbalances are observable in baseband I/Q symbols, it serves as a motivation to develop an alternative method for device identification. Our previous work has proposed an NN-based device identification with constellation pattern, which is formed by grouping I/Q symbols into their corresponding constellation points [9].

Although NNs generally handle input signals and weight coefficients in the real number domain, transmitted and received signals in communication systems are often represented in the complex number domain. In such cases, it is difficult for NNs in the real number domain to fully capture the inherent features of these signals in complex number domain. To address this, there exists a type of NN called a complex-valued neural network (CvNN), which is extended to operate in the complex domain [10] [11] [12]. CvNN, with its high generalization capability demonstrated in computer simulations, is a framework well-suited for handling the rotation and scaling of signals in the complex plane. It is gaining more attention in wireless communications, where it is essential to inherently deal with complex values.

In this study, we propose a CvNN-based device identifier, where multiple devices with their device-specific I/Q imbalance transmit signals to an access point (AP) in time-division multiple access, with the aim of enhancing the security of regular communications. The AP receives RF signals from each of the devices and down-converts them into baseband I/Q symbols. These symbols are grouped into the corresponding constellation points based on the coded bits estimated by the regular communication branch. The average of the symbols at each constellation point forms a constellation pattern that characterizes the device-specific I/Q imbalances. The CvNN-based device identifier recognizes this pattern to identify the device. The simulation results show that the identification

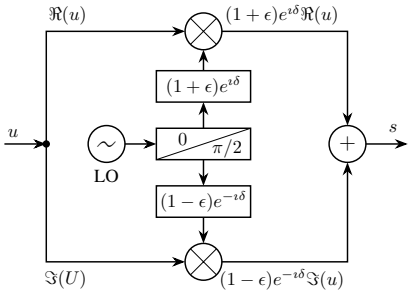

Fig. 1. A discrete-time model of the equivalent baseband signal for the modulator using direct up-conversion with I/Q imbalances

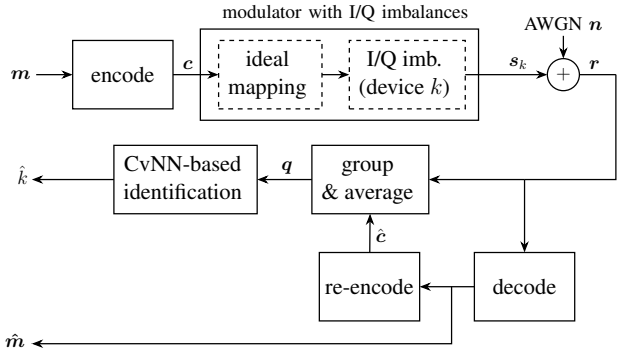

Fig. 2. Device identification system using CvNN

performance of the CvNN outperforms that of the real-valued neural network (RvNN), and approaches a lower bound of maximum likelihood identification. This is because CvNN captures the internet correlation in complex-valued I/Q symbols caused by I/Q imbalances.

II. I/Q Imbalances in Direct Up-Conversion Transmitter

This section reviews the model of I/Q imbalances in direct up-conversion transmitter.

We describe a transmitter signal model with I/Q imbalances (up-conversion). In this model, ϵ and δ represent the amplitude and phase imbalance distortions, respectively, and are modeled as random variables. $(1+\epsilon)$, $(1-\epsilon)$ and δ, $-\delta$ denote the amplitudes and phases of the I and Q branches, respectively. Let $u_{\mathrm{I}}(t)$ and $u_{\mathrm{Q}}(t)$ be the I and Q data signals to be modulated, and let ω_c be the frequency of the RF carrier. The transmitter output is given by

$$\begin{aligned} &u_{\mathrm{I}}(t)(1+\epsilon)\cos(\omega_c t+\delta) - u_{\mathrm{Q}}(t)(1-\epsilon)\sin(\omega_c t-\delta) \\ &= \Re\left(\left((1+\epsilon)e^{\imath\delta}u_{\mathrm{I}}(t) + \imath(1-\epsilon)e^{-\imath\delta}u_{\mathrm{Q}}(t)\right)e^{\imath\omega_c t}\right) \\ &= \Re\left(s(t)e^{\imath\omega_c t}\right) \end{aligned}$$

where

$$s(t) = (1+\epsilon)e^{\imath\delta}u_{\mathrm{I}}(t) + \imath(1-\epsilon)e^{-\imath\delta}u_{\mathrm{Q}}(t). \tag{1}$$

Here $s(t)$ is the equivalent complex baseband signal with I/Q imbalances, $u_{\mathrm{I}}(t) + \imath u_{\mathrm{Q}}(t) \triangleq u(t)$ is the complex data signal to be modulated, and $\imath = \sqrt{-1}$ is the imaginary unit.

The discrete-time representation of (1) is

$$s = (1+\epsilon)e^{\imath\delta}\Re(u) + \imath(1-\epsilon)e^{-\imath\delta}\Im(u) \triangleq \psi(\epsilon,\delta,u) \tag{2}$$

where u denotes the standard, complex modulation symbol. A modulator using direct up-conversion with I/Q imbalances is shown in Fig. 1.

For modulation of Q order, complex symbols $u_0, u_1, \ldots, u_{Q-1}$ comprise the set of standard modulation symbols $\mathcal{M}^0 = \{u_i\}_{i=0}^{Q-1}$. A standard modulation maps length-Q binary vector $\boldsymbol{d}$ to complex symbol u_i, where $\boldsymbol{d}$ is a binary representation of decimal i. Moreover, the Q points of u_i, $i = 0, 1, \ldots, Q-1$, form a standard constellation in the I-Q plane.

The modulation symbol set of a device affected by its specific I/Q imbalances becomes [13] [14]:

$$\mathcal{M} = \{s = \psi(\epsilon,\theta,u) | u \in \mathcal{M}^0\}. \tag{3}$$

The Q points of $s_i = \psi(\epsilon,\theta,u_i)$, $i = 0, 1, \ldots, Q-1$, form a constellation patten with I/Q imbalances at the I-Q plane.

The device-specific distortion due to I/Q imbalances arises from the alteration of amplitude and phase in the I and Q components, which are ideally orthogonal. Since I/Q impairments are hardware-specific and difficult to manipulate, they are utilized as device identification to secure IoT communications [2] [9]. Although the I/Q components in ideal modulation are orthogonal, the distortion leads to a correlation between the real and imaginary parts of the complex numbers (see 2). This encourages us to use CvNN for device identification by employing complex numbers as input.

III. Device Identification Using CvNN

This section discusses how the distinct constellation patterns caused by I/Q imbalances functions as a device identifier to enhance communication security. These patterns are recognized by employing a CvNN-based system for device identification.

A. System Model

The configuration of the system includes K devices and an AP. Define the set of devices as $\mathcal{K} = \{1, 2, \ldots, K\}$, with each device exhibiting distinct I/Q imbalances.

In Fig. 2, the AP receives coded modulation symbols from device $k \in \mathcal{K}$, estimates the message from device k, and identifies the device. Specifically, on the transmitting side of device k, the message bit sequence $\boldsymbol{m}$ is encoded into $\boldsymbol{c}$ with a channel code such as a polar code. Then, modulation is performed on the coded bit sequence in units of $\log_2 Q$ bits, and the sequence of modulation symbols $\boldsymbol{s}_k = (s_{k,0}, \ldots, s_{k,J-1})$, which is affected by the device-specific I/Q imbalances, is obtained. Here, $\mathcal{M}_k$ is the modulation symbol set of device k affected by its specific I/Q imbalances:

$$\mathcal{M}_k = \{s = \psi(\epsilon_k,\delta_k,u) | u \in \mathcal{M}^0\} \tag{4}$$

and $s_{k,j} \in \mathcal{M}_k$.

The modulated transmitted symbols $\boldsymbol{s}_k$ are subject to noise $\boldsymbol{z}$ in the communication channel, resulting in received symbols:

$$\boldsymbol{r} = \boldsymbol{s}_k + \boldsymbol{z}, \quad k \in \mathcal{K}. \tag{5}$$

Hear, each component in noise vector $\boldsymbol{z}$, denoted $z_j \sim \mathcal{CN}(0, \sigma^2)$, follows a circularly symmetric complex Gaussian distribution. Although the received symbols $\boldsymbol{r}$ contain slight distortions due to the transmitter's I/Q imbalances, reliable communication is achieved through channel coding and decoding, allowing the original message bits to be restored.

For device identification, we explain the formation of constellation patterns and the device identifier in sections III-B and III-C, respectively.

B. Formation of Constellation Patterns

For device identification, the estimated message bit sequence $\hat{\boldsymbol{m}}$ is re-encoded into a coded bit sequence $\hat{\boldsymbol{c}} = (\hat{\boldsymbol{d}}_0, \ldots, \hat{\boldsymbol{d}}_{J-1})$. According to the value of $\hat{\boldsymbol{d}}_j$, the AP groups the received symbols r_j by matching them to the ideal points within the constellation. The average at each point is calculated as:

$$q_i = \frac{1}{\sum_{j=0}^{J-1} \mathbb{I}_i(\hat{\boldsymbol{d}}_j)} \sum_{j=0}^{J-1} r_j \mathbb{I}_i(\hat{\boldsymbol{d}}_j), \quad i = 0, 1, \ldots, Q-1 \tag{6}$$

where $\mathbb{I}_i(\boldsymbol{d})$ is the indicator function defined as:

$$\mathbb{I}_i(\boldsymbol{d}) = \begin{cases} 1, & \text{if } \boldsymbol{d} \text{ is a binary representation of } i \\ 0, & \text{otherwise.} \end{cases} \tag{7}$$

The estimated constellation pattern $\mathcal{Q} = \{q_i\}_{i=0}^{Q-1}$, which remains as complex numbers, is inputted into a CvNN with input nodes Q.

C. Device Identifier

The CvNN uses the device-specific constellation pattern as input to identify the device. Since the constellation pattern is a complex vector, all inputs and parameters (weights, biases) of the CvNN are complex-valued. Moreover, activation functions are also complex functions.

The basic structure of CvNN consists of one input layer, N hidden layers, and one output layer. Each hidden layer in a CvNN unit is composed of a weight matrix W_j, a bias vector $\boldsymbol{b}_j$, and an activation function ϕ. The output layer is composed of a weight matrix W_o, a bias vector b_o, and an activation function ϕ_o. The output of the CvNN with N hidden layers is expressed as follows:

$$f(\boldsymbol{q}; \Theta) = \phi_o(W_o \phi_N(W_N \phi_{N-1}(\ldots \phi_1(W_1 \boldsymbol{q} + \boldsymbol{b}_1) \ldots) + \boldsymbol{b}_N) + \boldsymbol{b}_o), \tag{8}$$

where $\boldsymbol{q} = (q_0, q_1, \ldots, q_{Q-1})$ represents the input to the CvNN unit, and Θ is the set of weight matrices and bias vectors for the CvNN, i.e., $\Theta = \{W_j, \boldsymbol{b}_j | j = 1, \ldots, N\} \cup \{W_o, \boldsymbol{b}_o\}$.

In this study, two types of complex activation functions are used. The first is the complex rectified linear unit (CReLU), used in the hidden layers, and is defined as:

$$\begin{aligned} \phi(z) \triangleq \mathrm{CReLU}(z) &= \max(0, x) + \imath \max(0, y) \\ &= \begin{cases} z, & \text{if } x \geq 0 \text{ and } y \geq 0 \\ x, & \text{if } x \geq 0 \text{ and } y < 0 \\ \imath y, & \text{if } x < 0 \text{ and } y \geq 0 \\ 0, & \text{otherwise} \end{cases} \end{aligned} \tag{9}$$

where $z = x + \imath y$ is a complex number. The CReLU is a nonlinear function with a domain of $(-\infty, +\infty)$ and a range of $[0, +\infty]$.

The second activation function is the complex softmax function (Csoftmax), used in the output layer, and is expressed as:

$$\phi_o(z_l) \triangleq \mathrm{Csoftmax}(z_l) = \frac{\mathrm{softmax}(x_l) + \mathrm{softmax}(y_l)}{2} \tag{10}$$

$$\mathrm{softmax}(x_l) = \frac{e^{x_l}}{\sum_{m=1}^{L} e^{x_m}}, \quad \mathrm{softmax}(y_l) = \frac{e^{y_l}}{\sum_{m=1}^{L} e^{y_m}}$$

$$l = 1, \cdots, K,$$

where $z_l = x_l + \imath y_l$ is a complex number. The final prediction of the CvNN is the label k^* of the device with the highest probability, that is $\hat{k} \triangleq l^* = \arg\max_l \phi_o(z_l)$.

The parameters of the CvNN weight matrices and bias vectors Θ are generally obtained by calculating the loss between the CvNN output $\phi_o(\boldsymbol{z})$ and the labeled training data $\boldsymbol{t}$, then minimizing this loss. For this classification problem, cross-entropy loss is adopted as the loss function:

$$\begin{aligned} E(\phi_o(\boldsymbol{z}), \boldsymbol{t}) &= -\sum_{l=1}^{K} t_l \log \phi_o(z_l) \\ &\text{s.t. } \sum_{l=1}^{K} t_l = 1 \text{ and } \sum_{l=1}^{K} \phi_0(z_l) = 1. \end{aligned} \tag{11}$$

The parameters are updated to obtain the optimal output, using complex backpropagation and stochastic gradient descent (SGD) algorithms [10] [15] [16].

TABLE I
SIMULATION SPECIFICATIONS

Item	**Specification**
number of devices	10
CvNN structure	4-10-30-30-10
activation functions	CReLU, CSoftmax
loss function	cross-entropy
learning algorithm	SGD
learning rate	0.01
epochs	10
batch size	32
training SNR (dB)	35
symbols per device	20000 × 128
training data	10 × 20000 × 128
test data	10 × 20000 × 128

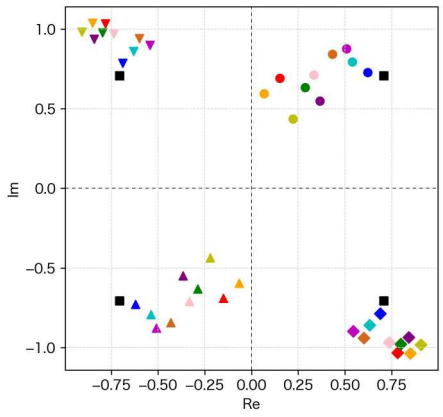

Fig. 3. $K = 10$ constellation patterns from modulation symbol sets $\mathcal{M}_k$, $k = 1, 2, \ldots, 10$, with device-specific I/Q imbalances

IV. Simulation Results

In this section, we provide the simulation results for the identification of K devices, following the methodology discussed in Section III.

A. Simulation Setup

We simulate the system consisting of an AP and $K = 10$ devices. The modulation scheme used is QPSK (with $Q = 4$ modulation symbols). The I/Q imbalance distortions, ϵ_k and δ_k are independent random variables that follow uniform distributions over the ranges $[\epsilon_{\rm L} = 0, \epsilon_{\rm U} = 0.3]$, $[\delta_{\rm L} = 0, \delta_{\rm U} = 30^\circ]$, respectively. Figure 3 shows the constellation patterns for each of the 10 devices simulated, which reflect their respective sets of modulation symbols affected by I/Q imbalances. The patterns are color-coded for each device. In addition, the power of the modulation symbols is normalized.

For channel coding, we used a polar code with a length of 256 bits and a coding rate of 0.5. In the AP, successive cancellation decoding is used for polar decoding [17].

The fully connected CvNN consists of an input layer with $Q = 4$ nodes, three ($N = 3$) hidden layers with 10, 30, and 30 nodes, respectively, and an output layer with $K = 10$ nodes. The activation function used in each node in hidden layers is the CReLU function of (9), while the output layer uses the CSoftmax function of (10). The CvNN's parameters are updated using the SGD algorithm. Table I shows the simulation specifications.

B. results

We trained the CvNN using the received data of the $10 \times 20,000 \times 128$ symbols at SNR of 35 dB, which are polar coded in the transmitters. Then we tested the average device identification error rate using another set of polar coded received data of $10 \times 20,000 \times 128$ symbols at different SNR values, with increments of 1 dB, as shown in Fig. 4.

For comparison, we also tested an RvNN (see Fig. 4), where the input was divided into real and imaginary parts, resulting in an input layer with 8 nodes. The structure of RvNN is the same as that of CvNN, with three hidden layers of 10, 30, and 30 nodes, and an output layer of 10 nodes. The RvNN parameters were also updated using the SGD algorithm.

As shown in Fig. 4, the identification error rate using CvNN is lower than that using RvNN. This is because, as discussed in Section II, the outputs of the I path and the Q path are correlated, which allows CvNN to capture the inherent correlation in complex-valued I/Q symbols. For example, in Fig. 5, the average correlation between the real and imaginary parts of the received complex symbols was found to be 0.45, indicating a strong correlation due to I/Q imbalances. In RvNN, on the contrary, a complex symbol is separated into its real and imaginary components, which are then processed separately. This disrupts the correlation between these components, leading to a decline in performance.

Furthermore, in Fig. 4, we calculate the identification error rate using the maximum likelihood (ML) method for comparison. This method calculates the Euclidean distance between the estimated constellation pattern $\mathcal{Q} = \{q_i\}_{i=0}^{Q-1}$ and the set of modulation symbols $\mathcal{M}_k$ ($k \in \mathcal{K}$), and identifies the device with the smallest distance. Although ML identification is not practical since the modulation symbol sets with I/Q imbalances are not directly observable, it serves as a lower bound.

To verify the polar decoding effect on the performance of the device identification system, we assume that demodulation is perfectly accurate. In other words, we assume that the values of $\boldsymbol{d}_j$ in (6) are successfully estimated. This is called ideal demodulation. Fig. 6 compares the results of device identification using polar decoding with those using ideal demodulation. The error rate appears to be marginally influenced by inaccuracies in polar decoding for both CvNN and RvNN, although it remains within an acceptable range.

Next, we consider a transmission of only $J = 4$ symbols

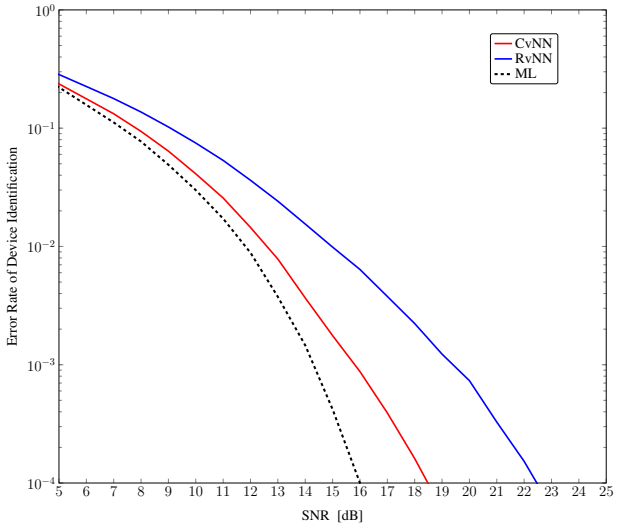

Fig. 4. Device identification using constellation patterns with I/Q imbalance (number of transmitted symbols: 128 symbols)

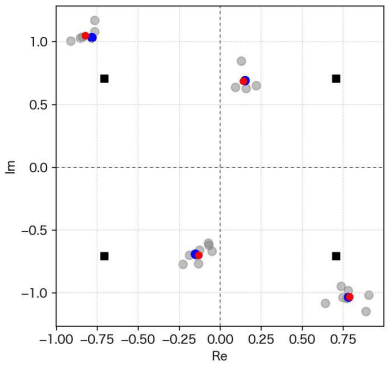

Fig. 5. An example of $J = 20$ received symbols of a device. Gray points: r_j, red points: q_i, $(i = 0, 1, 2, 3)$, forming a constellation pattern with I/Q imbalances, black squares: $u_i \in \mathcal{M}^0$, and blue points: $s_i \in \mathcal{M}_k$

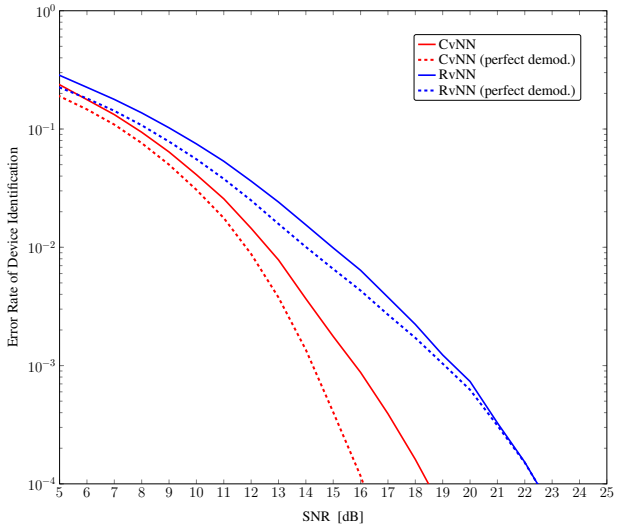

Fig. 6. Comparison with ideal demodulation (number of transmitted symbols: 128 symbols)

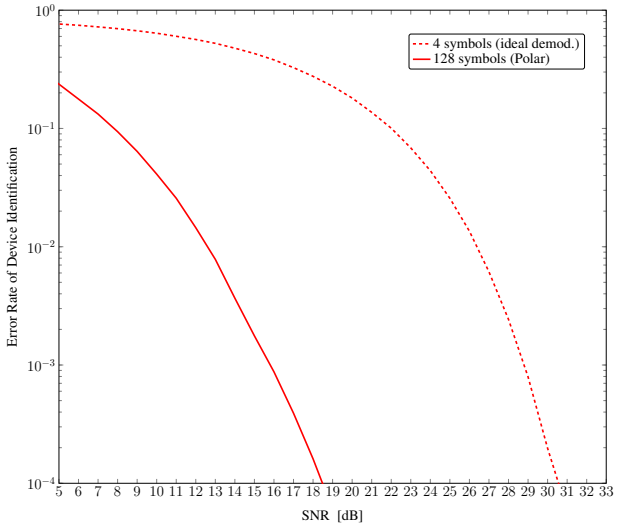

Fig. 7. Comparison by the number of transmitted symbols (4 symbols vs. 128 symbols)

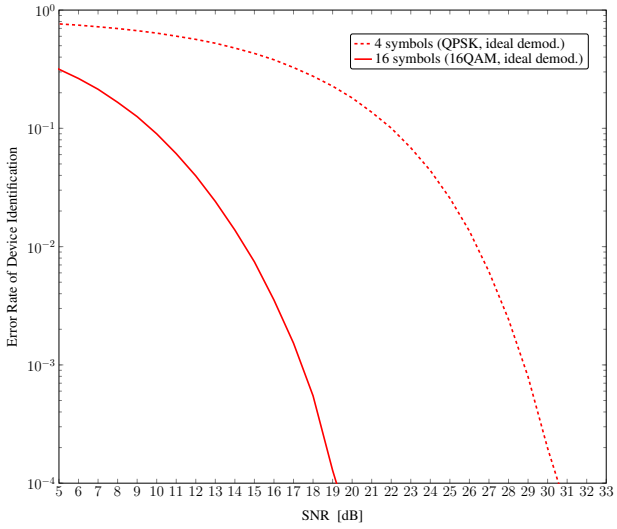

Fig. 8. Comparison of QPSK and 16QAM with an identical count of message bits

that include all symbols in $\mathcal{M}_k$ of QPSK. We compared the results of using the $J = 128$ transmitted symbols with using the transmission of the 4 symbols with ideal demodulation, as shown in Fig. 7. Comparison of results by the number of transmitted symbols confirms that increasing the number of symbols improves identification performance through processes such as averaging on the received symbols.

Finally, we conducted simulations using 16QAM, a higher-order modulation method, to compare it against the QPSK simulations performed thus far. The results are shown in Fig. 8. The comparison between QPSK and 16QAM reveals that 16QAM, being a higher-order modulation scheme, achieves lower identification error rate. This is likely because 16QAM has more features than QPSK, leading to improved identification performance.

V. Conclusion

We proposed a CvNN-based device identification to enhance the security of communications. Devices have I/Q impairments that arise from variations in the manufacturing process. An AP receives I/Q symbols from a device and forms a constellation pattern, which has a unique feature of the device's inherent I/Q impariments. The CvNN is able to recognize the device by categorizing the pattern. Simulations show that the CvNN has a lower error rate in identification than an RvNN. This is because the CvNN captures the inhenrent correlation in complex-valued I/Q symbols caused by I/Q imbalances.

Acknowledgements

The authors would like to thank Mr. Takahiro Higuchi for his valuable insights and suggestions during the research process.

REFERENCES

[1] E. Illi, M. Qaraqe, S. Althunibat, A. Alhasanat, M. Alsafasfeh, M. de Ree, G. Mantas, J. Rodriguez, W. Aman, and S. Al-Kuwari, "Physical layer security for authentication, confidentiality, and malicious node detection: A paradigm shift in securing iot networks," *IEEE Communications Surveys & Tutorials*, vol. 26, no. 1, pp. 347–388, 2024.

[2] J. Zhang, R. Woods, M. Sandell, M. Valkama, A. Marshall, and J. Cavallaro, "Radio frequency fingerprint identification for narrowband systems, modelling and classification," *IEEE Transactions on Information Forensics and Security*, vol. 16, pp. 3974–3987, 2021.

[3] Y. Shi and M. A. Jensen, "Improved radiometric identification of wireless devices using MIMO transmission," *IEEE Transactions on Information Forensics and Security*, vol. 6, no. 4, pp. 1346–1354, 2011.

[4] H. J. Patel, M. A. Temple, and R. O. Baldwin, "Improving ZigBee device network authentication using ensemble decision tree classifiers with radio frequency distinct native attribute fingerprinting," *IEEE Transactions on Reliability*, vol. 64, no. 1, pp. 221–233, 2015.

[5] J. He, S. Huang, S. Chang, F. Wang, B.-Z. Shen, and Z. Feng, "Radio frequency fingerprint identification with hybrid time-varying distortions," *IEEE Transactions on Wireless Communications*, vol. 22, no. 10, pp. 6724–6736, 2023.

[6] K. Youssef, L. Bouchard, K. Haigh, J. Silovsky, B. Thapa, and C. V. Valk, "Machine learning approach to RF transmitter identification," *IEEE Journal of Radio Frequency Identification*, vol. 2, no. 4, pp. 197–205, 2018.

[7] L. J. Wong, W. C. Headley, and A. J. Michaels, "Specific emitter identification using convolutional neural network-based IQ imbalance estimators," *IEEE Access*, vol. 7, pp. 33 544–33 555, 2019.

[8] L. Angrisani, M. D'Arco, and M. Vadursi, "Clustering-based method for detecting and evaluating I/Q impairments in radio-frequency digital transmitters," *IEEE Transactions on Instrumentation and Measurement*, vol. 56, no. 6, pp. 2139–2146, 2007.

[9] Y. Kitagawa, T. Higuchi, T. Kimura, and J. Cheng, "Neural network-based RF device identification with constellation pattern," in *2023 IEEE 9th World Forum on Internet of Things (WF-IoT)*, 2023, pp. 01–02.

[10] C. Trabelsi.et.al, "Deep complex networks," *arXiv:1705.09792v4*, p. 10, 2018.

[11] Y. Tu, Y. Lin, C. Hou, and S. Mao, "Complex-valued networks for automatic modulation classification," *IEEE Transactions on Vehicular Technology*, vol. 69, no. 9, pp. 10 085–10 089, 2020.

[12] S. Kim, H.-Y. Yang, and D. Kim, "Fully complex deep learning classifiers for signal modulation recognition in non-cooperative environment," *IEEE Access*, vol. 10, pp. 20 295–20 311, 2022.

[13] A. Mohammadian and C. Tellambura, "RF impairments in wireless transceivers: Phase noise, CFO, and IQ imbalance – A survey," *IEEE Access*, vol. 9, pp. 111 718–111 791, 2021.

[14] B. Razavi, *RF Microelectronics*. Prentice Hall, 1998.

[15] J. A. Barrachina, C. Ren, C. Morisseau, G. Vieillard, and J.-P. Ovarlez, "Complex-valued vs. real-valued neural networks for classification perspectives: an example on non-circular data," *ICASSP 2021 - 2021 IEEE International Conference on Acoustics, Speech and Signal Processing (ICASSP)*, pp. 2990–2994, 2021.

[16] K. Kreutz-Delgado, "The complex gradient operator and the $\mathbb{CR}$-calculus," 2009. [Online]. Available: https://arxiv.org/abs/0906.4835

[17] E. Arikan, "Channel polarization: A method for constructing capacity-achieving codes for symmetric binary-input memoryless channels," *IEEE Transactions on Information Theory*, vol. 55, no. 7, pp. 3051–3073, 2009.